Structure and defects of epitaxial $Cr_2O_3(0001)$ overlayers on Cr(110)

A. Stierle,* Th. Koll, and H. Zabel
Ruhr-Universität Bochum, Fakultät für Physik und Astronomie, Institut für Experimentalphysik/Festkörperphysik, D-44780 Bochum, Germany
(Received 3 November 1997)

The structure and defects of thin epitaxial $Cr_2O_3(0001)$ overlayers on Cr(110) films have been investigated by grazing incidence x-ray diffraction. Cr(110) films were prepared by molecular beam epitaxy before exposing them to a controlled oxygen atmosphere in the temperature range 400–800 K. The experiments reveal over the whole temperature range the same in-plane orientational relationship between $Cr_2O_3(0001)$ and Cr(110), which is a Nishiyama-Wassermann–type alignment between the oxygen sublattice and the Cr(110) surface. Out-of-plane measurements demonstrate the presence of growth and deformation faults within the Cr-ion and oxygen-ion sublattices. At higher temperatures mainly twin formation takes place, whereas at lower temperatures a random stacking of the Cr-ion layers prevails. We propose that the twin grain boundaries serve as diffusion channels for Cr ions during the oxidation. [S0163-1829(98)08931-0]

I. INTRODUCTION

Oxidation of metals is an everyday phenomenon. Depending on temperature, oxygen pressure, and time, oxide layers are formed on metals having different thicknesses and structural properties. The analysis of the oxide crystal structure, the epitaxial relationship to the metal substrate, and the defects formed during the oxidation process are therefore issues of fundamental interest. They determine the oxidation kinetics and the potentially protective character of the oxide layers. In this paper structural investigations of thin $Cr_2O_3(0001)$ films are described. Polycrystalline α-Cr_2O_3 layers play an important role as protective overlayers for stainless steels.[1] Up to now it is not clear whether the close-packed corundum structure of the Cr oxide layer or its chemical properties are responsible for the protective character of the oxide.

The surface aspects of oxidation seem to be well understood. First, oxygen is chemisorbed dissociatively on the metal surface and later on the growing oxide layer to enable a continuous oxide growth.[2,3] Second, a charge transfer has to take place from the metal/oxide interface to the oxide surface and ions need to diffuse through the growing oxide layer.[4–7] In a steady state these charge currents have to equilibrate. Depending on the conductivity of the oxide layer, either electron or hole conduction prevails. In the case of electron conduction the metal ions diffuse from the interface to the surface, whereas in the case of hole conduction the oxygen ions diffuse from the surface towards the interface. The processes occurring at the metal/oxide interface cannot be studied with standard surface science methods nor the overall structure of the oxide layer. Information on both is, however, essential for a detailed understanding of the growth mechanism.

In situ x-ray reflectivity studies of the Cr-oxide growth on Cr(110) have revealed a passivation of the surface for oxidation temperatures up to 700 K.[8] From 400 K to 700 K the oxide thickness increases very rapidly within the first few seconds (early growth stage), whereas after the following 1000 s the oxide growth increases very slowly (late growth stage). The oxidation kinetics of $Cr_2O_3(0001)$ on Cr(110) can be described quantitatively by assuming that the Cr-ion diffusion current controls the oxide growth. For the metal-ion diffusion an activation energy of 1.4 eV is found, which is a factor of 2 smaller than the bulk values.[8] Ion diffusion can take place via interstitial sites of the corundum lattice or via topological defects such as grain boundaries. Because of the low activation energy, Cr-ion diffusion via grain boundaries in the growing oxide layer appears more probable. The conclusion that the Cr ions are the diffusing species is also supported by chemical tracer[9] and nuclear tracer experiments.[6]

Up to ~725 K, the growth of the oxide layer is laterally very homogeneous. The surface and interface roughness are comparable to the initial Cr surface roughness.[10] Above 725 K a roughening of the oxide layer occurs. This roughening indicates that the ion diffusion current through the oxide layer (vertical diffusion) has suddenly become much stronger, exceeding the lateral diffusion current on the oxide surface. Since the metal-ion diffusion current proceeds along structural defects, the question arises how the structures and defects of the oxide layers differ above and below the roughening transition. Using grazing incidence x-ray diffraction (GIXD), which probes the in- and out-of-plane structure of the oxide layers,[11,12] some of the questions raised shall be answered in the following sections.

II. EXPERIMENTAL DETAILS

Single crystalline Cr(110) films were grown by molecular beam epitaxy (MBE) on $Al_2O_3(11\bar{2}0)$ substrates, using a Nb(110) buffer layer.[13,14] Typical thicknesses of the Nb(110) and the Cr(110) layer were about 20 nm each. The rms surface roughness of the Cr(110) layers routinely obtained was 0.2–0.4 nm, as determined by x-ray reflectivity measurements.[10,14] After growth, the samples were transferred from the MBE system into an ultrahigh vacuum (UHV) x-ray diffraction chamber, equipped with Be windows, sample heater, and oxygen inlet. During the sample transfer the sample was always kept under UHV conditions

and before the oxidation the clean Cr surface was studied. For each oxidation temperature a fresh sample was prepared and the oxidation was monitored by x-ray reflectivity measurements as a function of the oxidation time. The samples were oxidized at an oxygen pressure of 3.5×10^{-3} Pa for 1000 s. After the oxidation x-ray reflectivity scans provide the precise information on the oxide thickness grown, the surface and the metal/oxide interfacial roughness, and on the amount of Cr consumed by the oxide growth process.

After oxidation the samples were transferred back to the MBE chamber, where reflection high-energy electron diffraction (RHEED) and Auger electron spectroscopy provide complementary information. The in-plane structural information by RHEED examination can be compared to the results from GIXD measurements, which were carried out *ex situ*. *Ex situ* x-ray reflectivity measurements confirmed that the oxide thickness did not increase further when exposed to air. However, a small increase of the surface roughness of ~0.4 nm can be observed, which is probably due to the formation of carbonylic species on the surface.

GIXD measurements are highly sensitive to the in- and out-of-plane structures and to defects at the surface and in layers a few nanometers below the surface. In combination with *in situ* x-ray reflectivity measurements they are an ideal probe to characterize oxidation processes within the first few nanometers of oxide formed. A first set of data was taken using a grazing incidence x-ray diffractometer with horizontal scattering geometry installed at a laboratory rotating anode x-ray source.[15] The measurements were done using Cu $K\alpha$ radiation off a [0001] oriented graphite monochromator, allowing a separation of the $K\alpha$ and $K\beta$ lines. The incident beam had a divergence of 0.02° normal to the scattering plane in order to have a well defined incident angle α_i. The acceptance angle of the detector parallel to the surface was 1.2° for quick overview measurements. For a more quantitative analysis of Bragg peak positions and peak widths a higher resolution was achieved via a soller slit on the detector arm with an acceptance angle of 0.15°. The diffracted intensity had to be integrated over an exit angle from 0 to 2.5° to have a reasonable signal-to-noise ratio.

From these measurements the crystalline structure, the in-plane crystallite sizes, the mosaic distributions of the oxide layer, and the epitaxial relationships between the Cr(110) film and the oxide layer were determined. For the examination of the out-of-plane structure an intense synchrotron radiation source was used. The synchrotron experiments were carried out at the grazing incidence diffractometer of the wiggler beam line BW2 at the HASYLAB in z-axis geometry.[11] The angular acceptance of the detector was 1° normal to the surface and 0.07° parallel to the surface and a wavelength of 0.13051 nm was used.

III. IN-PLANE STRUCTURE

A. Cr_2O_3 on Cr(110)

Figure 1 shows the diffracted intensity as a function of the azimuthal sample angle ω (rotation axis normal to the surface) for Cr(110) films oxidized at different temperatures. The data were taken using the low-resolution setup described above. The scattering vector in the plane was kept fixed at a value of $Q=25.34$ nm^{-1} for the $\alpha-Cr_2O_3(11\bar{2}0)$ reflection. The incident angle was fixed at the critical angle of the oxide layer ($\alpha_i=0.31°$) in order to maximize the signal. The scans are displaced in the y direction by 1–2 orders of magnitude for clearer presentation. The counting time was 1 s for each point in all scans. The pseudosixfold symmetry observed here was also seen *in situ* with RHEED immediately after the oxide growth. Only the sample oxidized at 442 K did not produce a RHEED pattern, but the x-ray measurements detected already a faint diffraction pattern.

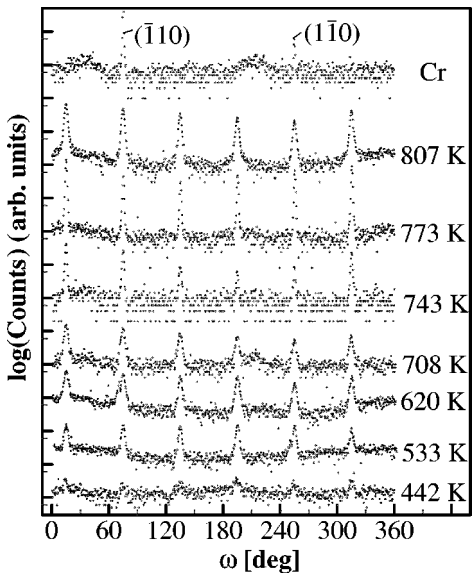

FIG. 1. Diffracted intensity as a function of the in-plane rotation angle ω for different oxidation temperatures. The scattering vector is fixed on the $Cr_2O_3(11\bar{2}0)$ reflection. In all scans six reflections appear, indicative of the pseudosixfold symmetry of the corundum (0001) planes. The topmost curve shows an ω scan on the $Cr(1\bar{1}0)$ reflection.

At all oxidation temperatures six reflections displaced by 60° in ω can be recognized. This is compatible with the pseudosixfold symmetry of the corundum (0001) planes. The intensity of the reflections increases with increasing oxidation temperature because the oxide thickness also increases from 1.9 nm at 442 K to 10.4 nm at 807 K.[8] The intensity variation of the reflections within one scan is due to the sample miscut and to geometrical effects. The background level for all measurements is ~10 counts/s, which is mainly due to diffuse scattering from the sample itself. The topmost curve reproduces an ω scan on the $Cr(1\bar{1}0)$ reflection with fixed $Q=30.62$ nm^{-1}. The two Cr reflections separated by 180° appear exactly at angular positions of the oxide reflections, which shows that the oxide layer and metal lattice are exactly aligned in this direction. The asymmetric intensity distribution of the Cr substrate reflections arises from the sample miscut.

In Fig. 2 radial scans in the $Cr_2O_3[11\bar{2}0]$ direction are shown for different oxidation temperatures. In the following we refer to directions in reciprocal space with square brackets, which are perpendicular to the corresponding Bragg planes written in parentheses. The measurements were done using the soller slit configuration to obtain a higher Q-space resolution. The data show the $Cr_2O_3(11\bar{2}0)$ reflection at $\simeq25.34$ nm^{-1}. The most prominent peak in all scans is the

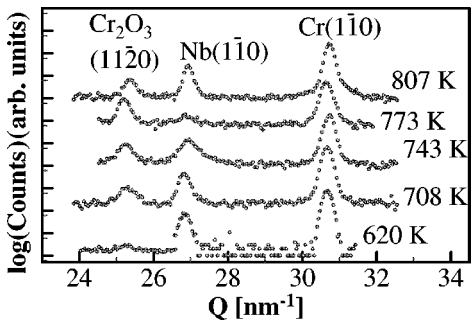

FIG. 2. Radial in-plane x-ray scans are shown under glancing incident angle conditions as a function of the magnitude of the scattering vector Q along the $Cr_2O_3(11\bar{2}0)$ direction and for different oxidation temperatures. The oxide peak intensity increases with the oxidation temperature because of increased oxide thickness and improved structural coherence of the oxide layer. Nb and Cr reflections from the substrate are also present.

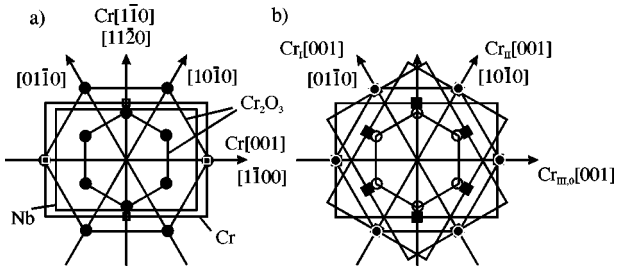

FIG. 4. (a) In-plane reciprocal lattice deduced from the x-ray scattering experiments after thermal oxidation of Cr(110) in the temperature range 400–800 K. Open squares denote the Cr and the filled circles the oxide reciprocal lattice points, respectively. The Nb reciprocal lattice is indicated by a solid line without points. (b) In-plane reciprocal lattice after additional deposition of Cr on the $Cr_2O_3(0001)$ layer. Open circles denote oxide and filled squares Cr reciprocal lattice points, respectively. Three independent (110) oriented Cr domains are formed on the oxide.

$Cr(1\bar{1}0)$ reflection at $Q \simeq 30.62$ nm^{-1}. This value shows a slight deviation from the Cr bulk value at $Q = 30.756$ nm^{-1}, which was verified by measurements on a Cr(110) single crystal in the same scattering geometry. The Cr(110) layer is expanded in the plane because of its epitaxy to the underlying Nb(110) layer.[13] The variation in the $Cr(1\bar{1}0)$ peak position as seen in Fig. 2 can be explained by different residual stresses in the Cr layers depending on their respective thicknesses.[13] The $Cr[1\bar{1}0]$ axis is found to be parallel to the $Cr_2O_3[11\bar{2}0]$ axis within 0.05°. The $Nb(1\bar{1}0)$ reflection at $Q = 26.93$ nm^{-1} shows a large variation in intensity, depending on the thickness of the Cr and the oxide layer, which first has to be penetrated before the Nb layer can be reached.

Equivalent oxide reflections are found in the $Cr_2O_3[1\bar{2}10]$ and $[2\bar{1}\bar{1}0]$ directions. In these directions the scans are free of metal reflections because of the twofold symmetry of the bcc(110) planes. Additional radial scans were taken in the $[10\bar{1}0]$ and equivalent directions. Figure 3 shows measurements for a sample oxidized at 773 K (oxide thickness 10.2 nm). The upper two curves were obtained in the $[1\bar{1}00]$ direction for two different angles of incidence.

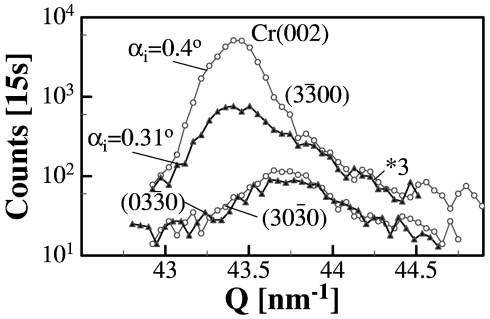

FIG. 3. Radial in-plane x-ray scans as a function of Q through the $(3\bar{3}00)$, $(03\bar{3}0)$, and $(30\bar{3}0)$ reflections. For the $[3\bar{3}00]$ direction a measurement with the incident angle at the critical angle ($\alpha_i = 0.31°$, open circles) of the oxide layer and above the critical angle ($\alpha_i = 0.4°$, solid line) is shown. At the critical angle the signal of the Cr(002) Bragg peak is reduced because of the limited penetration of the substrate.

They are both multiplied by a factor of 3 for clearer presentation. The Cr(002) reflection at $Q = 43.31$ nm^{-1} and the $Cr_2O_3(3\bar{3}00)$ reflection at 43.58 nm^{-1} overlap, giving direct evidence for the small lattice mismatch between the Cr and the Cr_2O_3 lattice in this direction. Decreasing the angle of incidence below the critical angle for the Cr layer, the signal from the Cr layer becomes less pronounced, yielding clearer evidence for the oxide signal. The oxide layer reflection can also be studied independently of the Cr(002) reflection if scans are taken along the $[01\bar{1}0]$ and $[10\bar{1}0]$ directions. The scans through the $(03\bar{3}0)$ and the $(30\bar{3}0)$ reflection of the oxide layer are shown in the lower part of Fig. 3.

The orientational relationship (OR) between Cr(110) and $Cr_2O_3(0001)$ determined over the whole oxidation temperature range 442–807 K can be summarized as follows: $Cr[1\bar{1}0] \| Cr_2O_3[11\bar{2}0]$, $Cr[001] \| Cr_2O_3[1\bar{1}00]$, and $Cr[110] \| Cr_2O_3[0001]$. The corresponding reciprocal in-plane lattice is plotted in Fig. 4(a). The filled circles mark the Cr_2O_3 reflections and open squares the Cr reflections. The Nb reciprocal lattice is indicated only by a solid line without reciprocal lattice points. The lattice mismatch between bulk $Cr_2O_3(0001)$ and Cr(110) films in the $[1\bar{1}00]$ direction is only 1.15%, explaining the good epitaxy between both structures.

The OR between the oxygen ion sublattice and the Cr(110) surface can be considered as to of the Nishiyama-Wasserman (NW) type. Theoretical calculations of the interfacial energy between bcc(110)/hexagonal closed packed (0001) layers reveal an energy minimum for $R_{bcc}/R_{hcp} = 0.866$,[16] where R is the atomic diameter in the hard sphere model. Assuming an O^{2-} ion radius of 0.14 nm and a Cr metal atom radius of 0.125 nm, the atomic diameter ratio between $Cr_2O_3(0001)$ and Cr(110) is 0.89, which is close to the minimum for the ideal NW OR. For the Cr^{3+} ion radius of 0.062 nm the ratio R_{bcc}/R_{hcp} is 2 and a Cr/Cr^{3+} interface is energetically much less favored. The realization of the NW OR indicates thus that the oxide layer is terminated by a close packed oxygen ion layer at the metal/oxide interface. A sharp metal/oxide transition at the interface is also favored by the small interfacial roughness of 0.2–0.4 nm that was deduced from reflectivity measurements

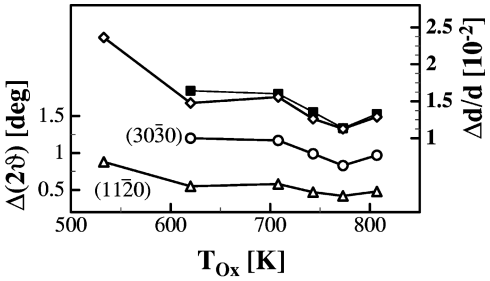

FIG. 5. Left axis, in-plane oxide radial peak width (FWHM) determined from the $(11\bar{2}0)$ and equivalent reflections (open triangles) and the $(30\bar{3}0)$ and equivalent reflections (open circles) as a function of the oxidation temperature; right axis, strain distribution for the $(11\bar{2}0)$ (open diamonds) and $(30\bar{3}0)$ (filled squares) directions as a function of the oxidation temperature.

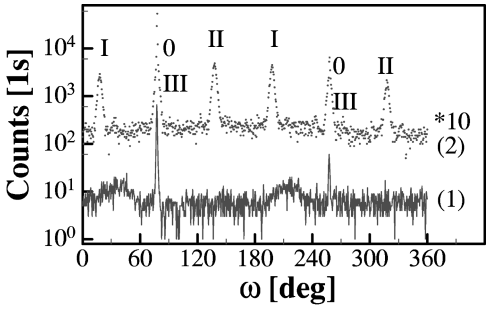

FIG. 6. In-plane ω scans with the scattering vector fixed on the $Cr(1\bar{1}0)$ reflection. Measurement (1) was obtained before deposition of Cr on the $Cr_2O_3(0001)$ layer and measurement (2) after deposition of 6 nm of Cr. The broad intensity distributions in (1) are due to shadowing effects of the background by the rectangular sample shape. Additional reflections appear after deposition because of the formation of three Cr domains on the oxide surface.

for oxidation temperatures below the roughening transition at ~ 725 K.[8,10] At higher temperatures a pore formation can be observed after the formation of 10 nm thick oxide layers, which we attribute to the quick material consumption from the metal oxide interface.[10] Nevertheless, we believe that in the initial stage of the high-temperature oxidation the same type of abrupt interface is present, which is washed out during further oxidation.

The OR observed here over a whole temperature range was reported before at more specific temperatures. Watari[17] and Michel and Jardin[18] describe the same OR after oxidation at 723 K and 1123 K, respectively. However, in contrast to Watari,[17] a spinel-like phase was not identified in the present study. Recently, Zhang *et al.* reported the growth of Cr_2O_3 on Pt(111), showing also a spinel-like structure in the early growth stage possibly induced by the Pt(111) substrate.[19] At larger thicknesses the authors observe the growth of α-Cr_2O_3 in the [0001] direction. Kennett and Lee detect the same OR after oxidation at 900 K and oxygen exposures above 10^{-4} Torr s.[20] Other OR's reported by these authors for oxidation temperatures between 570 K and 900 K and after lower oxygen exposures could not be reproduced in the present study.

For a more quantitative analysis of the structural perfection of the oxide layer the radial width of the oxide Bragg peaks was evaluated. In Fig. 5 the oxide in-plane radial 2ϑ peak width (left axis) is plotted. Each point represents the average over the widths from the three independent in-plane directions. The triangles mark the peak width obtained from the scans through $(11\bar{2}0)$ and equivalent reflections, the circles the ones from the $(30\bar{3}0)$ and equivalent reflections. The solid lines are guides to the eye. For both orientations the peak width decreases with the oxidation temperature and tends to saturate above 773 K at 0.4° for the $(11\bar{2}0)$ reflections, which corresponds to a virtual domain size of 20 nm using the Debye-Scherrer formula.[21] This value is not limited by the structural coherence of the underlying Cr layer, which was found to be larger than 40 nm.

An interesting point to note is the fact that the peak width of the $(30\bar{3}0)$ reflections is much bigger than the one from the $(11\bar{2}0)$ reflections. This can be taken as an indication of a peak broadening due to a strain distribution in the films. Assuming an average d-spacing distribution Δd, the peak broadening can be calculated simply by differentiation of Bragg's law: $\Delta 2\vartheta = -2\tan(\vartheta)\Delta d/d$. In Fig. 5 (right y axis) the relative strain distribution $\Delta d/d$ is plotted as a function of the oxidation temperature. The open diamonds correspond to the $(11\bar{2}0)$ reflections and the filled squares to the $(30\bar{3}0)$ reflections. The values are consistent for both orientations over the whole temperature range studied here, which shows that inhomogeneous strain is probably the main cause of peak broadening in this case. As an origin for inhomogeneous strain in-plane grain boundaries may act, as well as misfit dislocations, the latter being present because of the epitaxial growth.

In addition, the in-plane mosaicity was evaluated by the transverse widths of the reflections in ω scans. A decrease of the mosaicity can be observed above 700 K from about 3° to 1°, in accordance with the reduction of inhomogeneous strain of the films at higher temperatures.

B. Cr on $Cr_2O_3(0001)$

To understand the general nature of the epitaxy between Cr(110) and $Cr_2O_3(0001)$, the growth of Cr on a $Cr_2O_3(0001)$ layer was studied. The oxide layer had been prepared beforehand by oxidation of Cr(110) at 620 K. At this temperature smooth oxide films with sufficiently high in-plane order are obtained. After the *ex situ* measurement of the in-plane structure the sample was transferred back into the MBE chamber. After annealing at 1000 K for 30 min, 6 nm of Cr was deposited at a substrate temperature of 773 K and at a rate of 0.02 nm/s. Figure 6 shows the ω scans at $Q = 30.62$ nm^{-1} for the $Cr(1\bar{1}0)$ reflection before (1) and after (2) the Cr deposition using the low resolution setup. Before Cr deposition, the Cr substrate reflections separated by 180° can be recognized. Afterwards, a total of six broader reflections are present, separated by 60°, which are superimposed on the much sharper reflections of the Cr substrate layer. The reciprocal lattice related to the additional Cr overlayer is summarized in Fig. 4(b).

The Cr overlayer forms three domains labeled in Fig. 6 with I, II, and III. They have roughly equal occupation probability on the $Cr_2O_3(0001)$ surface, as can be judged from the equal Bragg intensities. Domain III is oriented along the

initial Cr$[1\bar{1}0]$ direction and the reflections overlap with the sharp substrate reflections (domain 0). Domains I and II are rotated by $\pm 60°$ with respect to domain III. This implies that, aside from the domain formation, the same OR can be found for the growth of Cr on $Cr_2O_3(0001)$ as vice versa. In addition, high-resolution measurements with a soller slit show that the Cr domains have the same mosaic distribution as the underlying oxide layer. The strain distribution obtained from radial scans through the Cr$(1\bar{1}0)$ overlayer reflections is $\Delta d/d = 1.6\%$, which is the same for the oxide layer substrate that was annealed 1000 K. This means that defects in the oxide layer such as grain boundaries are reproduced in the top Cr layer. This has the intriguing implication that on each oxide domain only one of the three possible Cr domains grows. The observation can be explained by assuming a nucleation site density within the first Cr layer, which is equal to or smaller than the density of oxide domains. In this case the Cr islands would grow laterally until they reach the border of the underlying oxide domain and the oxide domain structure is replicated by the growing metal film.

IV. ROD MEASUREMENTS

The measurements described in the preceding section considered only the in-plane structure of the oxide films. Additional information is required to complete the structural model and to characterize out-of-plane defects. For this reason measurements were performed in a crystal truncation rod mode, providing an additional momentum transfer perpendicular to the surface.[11,12] Before reporting the experimental results, a brief summary of the corundum reciprocal lattice and its description in terms of stacking sequences of dense packed layers may be in order.

A. Reciprocal lattice of the corundum structure

The bulk structure of α-Cr_2O_3 in the [0001] direction is composed of hexagonal close packed O^{2-} ion layers forming a hcp stacking sequence such as $ABAB\ldots$. The oxygen ion planes are alternating with buckled Cr ion planes, in which only 2/3 of the possible octahedral sites are filled.[22] Looking at a projection in the $[11\bar{2}0]$ direction, every third row of Cr^{3+} ions is missing and three different places for the missing atomic row are possible within the unit cell, as pictured in Fig. 7(a). This is equivalent to an $abcabc\ldots$ fcc-like stacking of the Cr ion layers. Together with the $AB\ldots$ stacking of the oxygen ion planes the total stacking sequence of the structure is given by $AaBbAcBaAbBc$, which explains the large repeat distance of 1.3584 nm for the Cr_2O_3 unit cell in the c direction.[22] The 2/3 filling of the Cr ion layers provokes a distortion of the oxygen sublattice, which will affect the absolute values for the x-ray structure factor.

The structure factor for the corundum structure can be calculated in the standard fashion.[21] For $h=0$ or $k=0$ only reflections with even Miller indices l in the [0001] direction are allowed. In this case the structure factor S can be written as

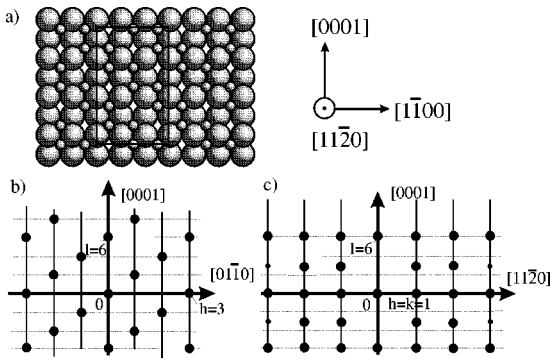

FIG. 7. Model of the Cr_2O_3 structure and out-of-plane reciprocal lattice. (a) Projection of the lattice in the $[11\bar{2}0]$ direction, where every third row of Cr^{3+} ions is missing, giving rise to an $abcabc\ldots$ fcc-like stacking of the Cr ion layers. The box shows one unit cell. (b) In the $[0001]/[01\bar{1}0]$ plane a fcc-like reciprocal lattice is present. (c) In the $[0001]/[11\bar{2}0]$ plane a hcp-like reciprocal lattice is present. The small circles correspond to reflections that are directly sensitive to the displacement of the ions in the corundum lattice away from the ideal hcp positions. The size of the symbols is *not* proportional to the structure factor.

$$S=\{4f_{\mathrm{Cr}}\cos 2\pi ul \pm 2f_{\mathrm{O}}[\cos 2\pi\nu h+\cos 2\pi\nu k+\cos 2\pi\nu(h+k)]\}\times\left(1+2\cos\pi h\cos\pi k\cos\frac{\pi}{3}(h-k-l)\right). \quad (1)$$

Here f_{Cr} describes the form factor of Cr^{3+}, f_{O} describes the form factor of O^{2-}, and ν,u are relative positions of the Cr and the oxygen ions, respectively. For an ideal hexagonal lattice, $\nu=u=1/3$; However, for Cr_2O_3 these values are $\nu=0.306$ and $u=0.3475$.[22] The ''+'' case in Eq. (1) holds for $l=0,4,8,\ldots$ and the ''−'' case for $l=2,6,10\ldots$.

If both h and $k\neq 0$, Bragg reflections having odd l values can also be exited. They arise from the oxygen ion sublattice only and their structure factor can be evaluated as

$$S=2f_{\mathrm{O}}[\sin 2\pi\nu(h+k)-\sin 2\pi\nu h-\sin 2\pi\nu k]\times\left(1-2\cos\pi h\cos\pi k\cos\frac{\pi}{3}(h-k-l)\right). \quad (2)$$

Furthermore, for $h=k\neq 0$ only reflections for even $l=6,12,\ldots$ can be observed and their structure factor is calculated by Eq. (1).

In Fig. 7(b) the partial reciprocal lattice spanned by the $[01\bar{1}0]$ and the [0001] direction is plotted. Obviously the reciprocal lattice cannot be transformed into itself by a rotation of 180° about the [0001] axis due to the threefold symmetry of the system. The corundum reciprocal lattice plane can be compared with the reciprocal lattice of a [111] oriented fcc structure where equivalent reflections have a nonvanishing structure factor. The fcc reciprocal lattice in this plane is sensitive to the layer stacking and stacking faults of subsequent layers as was shown, for instance, for the phase transition of hcp Co(0001) to fcc Co(111).[23,24]

Similar considerations hold for the corundum reciprocal lattice spanned by the $[11\bar{2}0]$ and the [0001] direction [see Fig. 7(c)]. Looking at a simple hcp reciprocal lattice com-

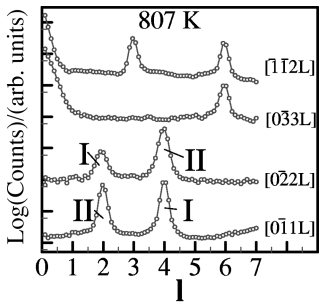

FIG. 8. Rod scans with synchrotron radiation as a function of the relative coordinate l in different oxide reciprocal lattice directions normal to the surface. The oxide layer was prepared by oxidation at 807 K. On the $[0\bar{1}1l]$ and the $[0\bar{2}2l]$ rod reflections at $l=2$ and 4 are observed, indicative for twin formation. For further details see text.

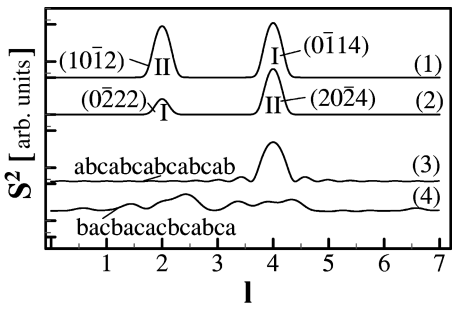

FIG. 9. Model calculations of the diffracted intensity along reciprocal lattice rods shown in Fig. 10. (1) and (2) Intensities along $[10\bar{1}l]$ and $[0\bar{2}2l]$ according to the ideal corundum lattice and assuming two domains with equal probability for $abca\ldots$ and $cbac\ldots$ stacking. (3) shows the intensity distribution along the same reciprocal lattice rod for 14 close-packed planes with only one domain of perfect stacking and (4) with completely random stacking.

posed of the hcp [0001] and $[10\bar{1}0]$ directions, nearly complete equivalence can be found. The reflections with corundum indices $(33\bar{6}3)$, $(66\bar{1}23)$, . . . or $(33\bar{6}9)$, $(33\bar{6}15)$ can only be seen in the corundum structure because of the distortion of the oxygen sublattice. In analogy to the previous case, the reciprocal lattice in this plane is only sensitive to the $ABAB\ldots$ stacking of the oxygen ion sublattice.

B. Experimental results

Rod scans have been performed on 10.4 and 3.2 nm thick oxide layers prepared by oxidation of Cr(110) at 807 K and 533 K, respectively. Figure 8 shows the diffracted intensity of four nonequivalent rods as a function of the reciprocal lattice coordinate l for the sample oxidized at 807 K. $l=1$ corresponds to the reciprocal lattice unit $|\vec{c}^*|=2\pi/c_0=4.6243\ \text{nm}^{-1}$.

The scans are offset by factors of 10 for clearer presentation. The $[\bar{1}\bar{1}2l]$ rod is sensitive to the stacking of the oxygen ion layers. The pure in-plane reflection occurs near $l=0$, followed by reflections at $l=3$ and 6, as expected for the $ABAB\ldots$ stacking of the oxygen ion layers. The full width at half maximum (FWHM) of the reflections, $\Delta l=0.25$ in relative units, corresponds to a stacking correlation length D of 5.4 nm in real space using the rough estimate $\Delta l=2\pi/D$. This value is about half of the total film thickness of 10.4 nm. The peak broadening is related to deformation and twin faults in the hcp stacking, such as $ABABCACA\ldots$ and $ABABCBCBC\ldots$, respectively.[21]

The $[0\bar{1}1l]$ and the $[0\bar{2}2l]$ rods are sensitive to the stacking of the Cr ion layers. In both scans we observe reflections at $l=2$ and 4. This contradicts the bulk structure factor, where only reflections at $l=4$ on the $[0\bar{1}1l]$ rod and at $l=2$ on the $[0\bar{2}2l]$ rod are expected. The presence of both reflections in one scan is a typical sign for twin formation, where domains with $abcabc$ and inverted $cbacba$ stacking sequences laterally coexist. The reflections assigned ''I'' can be attributed to $abcabc\ldots$ stacked domains and ''II'' corresponds to the $cbacba\ldots$ stacked domains. In these scans also a broadening of the reflections is present due to deformation and growth faults within each type of domain. In addition, these structural defects give rise to diffuse intensity between the reflections at $l=2$ and 4.[24] Again a stacking correlation of 5.5 nm can be deduced from the peak width of the $[0\bar{1}0l]$ rod.

For the bulklike, thicker oxide film, the scattered intensity can be calculated and compared to the measured intensities using the bulk structure factor. This will provide information on the occupation probability of the two stacking domains. The structure factor was calculated according to Eq. (1) and assuming that both stacking sequences have the same probability. Furthermore, all geometrical and Lorentz-polarization corrections necessary for the z-axis geometry were taken into account.[11] In Fig. 9 the calculated intensity is plotted (in relative units) as a function of l [curves (1) and (2)]. The plots are displaced by one order of magnitude. The intensity ratios of the reflections at $l=2$ and 4 are in very good agreement with the measured ratios seen in Fig. 8, confirming the equal probability of the two stacking domains, to be discussed further below. It would be of considerable interest to determine the density of twin (α) and deformation faults (β) from the broadening of the reflections. This is indeed possible for bulk fcc and hcp crystals and different calculations exist to connect the peak broadening with faulting probabilities, assuming infinite systems and small values for α and β.[21,24,25] However, these expressions cannot be applied to thin films because the above-mentioned conditions are not fulfilled.

Figure 10 shows the same measurements for the thinner

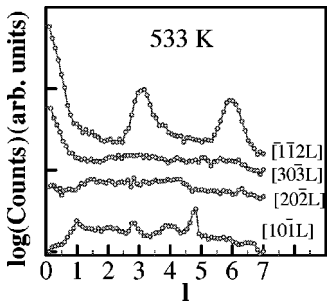

FIG. 10. Rod scans as a function of l for a sample oxidized at 533 K. The broad intensity modulation on the $[10\bar{1}l]$ and the $[20\bar{2}l]$ rod is produced by stacking faults of the Cr ion layers.

sample prepared by oxidation at 533 K. The scans are displaced by a factor of 5 for clearer presentation. Obviously the $[\overline{1}\overline{1}2l]$ rod shows again the reflections near $l=0$ and at $l=3$ and 6, corresponding to the *ABAB* hcp stacking of the oxygen ion layers. The peak width of $\Delta l=0.68$ indicates a stacking correlation length of 2 nm, compared to the total film thickness of 3.2 nm. In contrast to the sample prepared at higher temperatures, no reflections occur along the $[10\overline{1}l]$ and $[20\overline{2}l]$ rods. Only a broad intensity distribution is present. The sharp feature along the $[10\overline{1}l]$ rod is perhaps due to a substrate reflection. A broad intensity distribution along the $[10\overline{1}l]$ and $[20\overline{2}l]$ rods is due to a completely random stacking of the Cr ion layers as shown below. Also the reflection near $l=0$ on the $[30\overline{3}l]$ rod is always present, indicative of in-plane structural order independent of the growth temperature. The reflection at $l=6$ does not exist in the 533 K sample, which is another clear sign for the large amount of out-of-plane disorder in the Cr ion sublattice.

From a more qualitative point of view, it is clear that the deformation and twin faults in the Cr ion sublattice seem to be very high in the 533 K grown sample, causing a complete disappearance of the reflections sensitive to the fcc-like *abc* . . . stacking sequence. They exist, however, in the oxide film grown at higher temperatures. On the other hand, the *AB* . . . stacking of the oxygen ion layers is well developed for low and high oxidation temperatures, as can be recognized from the $[\overline{1}\overline{1}23]$ and $[\overline{1}\overline{1}26]$ reflections.

To show qualitatively that a high density of stacking faults in a thin layer can produce very broad intensity distributions, the ideal structure factor for 14 monolayers with perfect *abc* . . . stacking sequence is compared in Fig. 9 [curve (3)] with a structure factor for a stacking sequence containing an equal amount of twin and deformation faults [curve (4)]. In curve (3) the expected peak for the ideal structure at $l=4$ can be recognized, which is accompanied by finite film thickness oscillations. For the nonideal stacking sequence the intensity is smeared out over the entire *l* range and no clear peaks can be identified.

V. DISCUSSION AND CONCLUSIONS

In this work it was shown that epitaxial growth of $Cr_2O_3(0001)$ on Cr(110) by oxidation of a (110) oriented Cr film is possible over the whole temperature range from 400–800 K. X-ray investigations of the out-of-plane oxide structure reveal for high oxidation temperatures the following main defect types: two laterally separated stacking domains with inverted stacking sequence of the Cr ion layers occurring with about equal probability and in addition a small amount of stacking faults within each Cr-oxide domain. At oxidation temperatures at and below 533 K randomly stacked Cr-ion layers are identified, coexisting with a well ordered *ABAB* . . . stacking of the oxygen ion sublattice.

The twin formation at higher temperatures may be a consequence of the heteroepitaxial growth of $Cr_2O_3(0001)$ on Cr(110) and may already be implemented during the early growth stages. Figure 11(a) shows schematically the bcc Cr(110) surface with its two types of hollow sites, indicated as site 1 and site 2. Using both sites, two types of oxygen ion domains can be formed on the surface. Since these domains

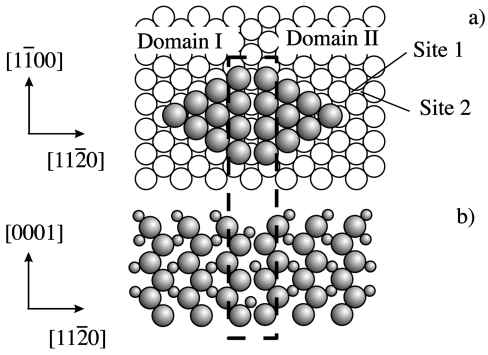

FIG. 11. Model for the domain formation during the oxidation: (a) top view of oxygen islands occupying different sites on the Cr(110) surface and (b) side view of the oxide layer; the domain grain boundaries can serve as channels for Cr ions for diffusion from the metal/oxide interface to the surface during oxide growth.

are displaced against each other, they cannot grow easily together. This is also shown by the side view of the structure in Fig. 11(b), where the two domains are sketched after formation of a certain oxide thickness. The grain boundary between the two domains can be used very effectively as a diffusion path for Cr ions from the interface to the surface during oxidation.

The oxide growth can develop independently for each oxygen ion domain. Cr ions, which diffuse on the surface of the first oxygen ion layer, may populate any of the three different configurations *a*, *b*, or *c* known from the bulk structure. The stacking sequence within one domain is fixed after chemisorption of the second oxygen-ion layer. If the first Cr-ion layer was grown in the *a* configuration, the second one can be grown in the *b* configuration according to the regular *abcabc* . . . stacking or in the *c* configuration, which corresponds to the inverted *acbacba* . . . stacking sequence. This argument holds also for domains that are starting with a Cr-ion layer in the *b* or the *c* configuration. If the temperature is high enough, the stacking sequence is maintained for each oxide crystallite during further oxide growth because the diffusion coefficient for Cr ions on the oxide surface is high enough to find the proper bulk positions. At lower temperatures, however, the Cr ions have a high probability to be stuck in nonbulk positions and a large number of stacking faults may accumulate. The increase of the in-plane oxygen domain size as a function of the oxidation temperature is probably due to the enhanced diffusivity of the oxygen ions on the Cr(110) surface. With increasing temperatures larger oxygen ion domains are formed, which leads to an increase of the in-plane domain size and the decrease of the in-plane inhomogeneous strain as discussed in Fig. 5. The in-plane domain size is maintained during further *z*-axis growth of the oxide crystallites at a certain temperature.

From our previous results[10] it can be concluded that smooth Cr_2O_3 layers can be grown by thermal oxidation of Cr(110) at lower temperatures (533 K) containing a significant amount of stacking faults in the Cr ion sublattice. Above the roughening transition at 725 K much rougher oxide layers with a nearly perfect Cr ion stacking sequence are formed. The main imperfection of these layers is the formation of twin domains with inverted Cr ion stacking sequences. Measurements of a sample oxidized at 620 K (be-

low the roughening temperature, not shown here) already exhibit an improved crystalline structure, but the same twin domains. This temperature can be chosen as a compromise between surface roughness and crystallinity to form Cr_2O_3 layers that can be used as substrates for other surface science experiments. Twin formation, however, cannot be avoided and seems to be inherently connected to the heteroepitaxial growth of $Cr_2O_3(0001)$ on Cr(110).

For the deposition of Cr(110) on a $Cr_2O_3(0001)$ layer, previously prepared by oxidation of Cr(110) at 620 K, epitaxial growth can be observed with the same OR's as for the growth of Cr_2O_3 on Cr(110). This opens the intriguing possibility for growing Cr/Cr_2O_3 superlattices by Cr deposition followed by controlled oxidation.

ACKNOWLEDGMENTS

We would like to thank M. Nielsen and R. Feidenhans'l from the Risø National Laboratory, Roskilde, Denmark for their help with the rod measurements. This work was supported by the Deutsche Forschungsgemeinschaft within the Graduiertenkolleg ''Dynamische Prozesse an Festkörperoberflächen: Adsorption, Reaktion, Heterogene Katalyse.''

*Present address: European Synchrotron Radiation Facility, Boîte Postale 220, 38043 Grenoble, France.

[1] J. C. Colson and J. P. Larpin, MRS Bull. **10**, 23 (1994).
[2] M. Henzler and W. Göpel, *Oberflächenphysik des Festkörpers* (Teubner, Stuttgart, 1991).
[3] A. Zangwill, *Physics at Surfaces* (Cambridge University Press, Cambridge, 1988).
[4] A. T. Fromhold, Jr. and Earl L. Cook, Phys. Rev. **158**, 600 (1967).
[5] A. T. Fromhold, Jr. and Earl L. Cook, Phys. Rev. **163**, 650 (1968).
[6] A. Atkinson, Rev. Mod. Phys. **57**, 437 (1985).
[7] F. H. Stott, Rep. Prog. Phys. **50**, 861 (1987).
[8] A. Stierle and H. Zabel, Europhys. Lett. **37**, 365 (1997).
[9] A. Stierle and H. Zabel, Surf. Sci. **385**, 310 (1997).
[10] A. Stierle and H. Zabel, Surf. Sci. **385**, 167 (1997).
[11] R. Feidenhans'l, Surf. Sci. Rep. **10**, 105 (1989).
[12] I. K. Robinson and D. J. Tweet, Rep. Prog. Phys. **55**, 599 (1992).
[13] P. Sonntag, W. Donner, N. Metoki, and H. Zabel, J. Appl. Phys. **73**, 4808 (1993).
[14] A. Stierle, P. Bödeker, and H. Zabel, Surf. Sci. **327**, 9 (1995).
[15] N. Metoki, W. Donner, and H. Zabel, Phys. Rev. B **49**, 17 351 (1994).
[16] E. Bauer and J. H. van der Merwe, Phys. Rev. B **33**, 3657 (1986).
[17] F. Watari, Surf. Sci. **110**, 111 (1981).
[18] P. Michel and Ch. Jardin, Surf. Sci. **36**, 478 (1973).
[19] L. Zhang, M. Kuhn, and U. Diebold, Surf. Sci. **375**, 1 (1997).
[20] H. M. Kennett and A. E. Lee, Surf. Sci. **33**, 377 (1972).
[21] B. E. Warren, *X-Ray Diffraction* (Dover, New York, 1990).
[22] R. W. G. Wyckoff, *Crystal Structures* (Intersciences, New York, 1963).
[23] F. Frey, W. Prandl, J. Schneider, C. Zeyen, and K. Ziebeck, J. Phys. F **9**, 603 (1979).
[24] T. Sebastian and P. Krishna, Phys. Status Solidi A **101**, 329 (1987).
[25] S. Hendricks and E. Teller, J. Chem. Phys. **10**, 147 (1942).